Supplemental Information

Microbuckling of Fibrin Provides a Mechanism for Cell Mechanosensing

Jacob Notbohm[1*], Ayelet Lesman[2], Phoebus Rosakis[3], David A. Tirrell[2], Guruswami Ravichandran[1]

[1]Division of Engineering and Applied Science, California Institute of Technology, Pasadena, CA 91125
[2]Division of Chemistry and Chemical Engineering, California Institute of Technology, Pasadena, CA 91125
[3]Department of Theoretical and Applied Mathematics, University of Crete, Heraklion 70013, Greece
* Correspondence to jknotbohm@wisc.edu

Supplemental Figures

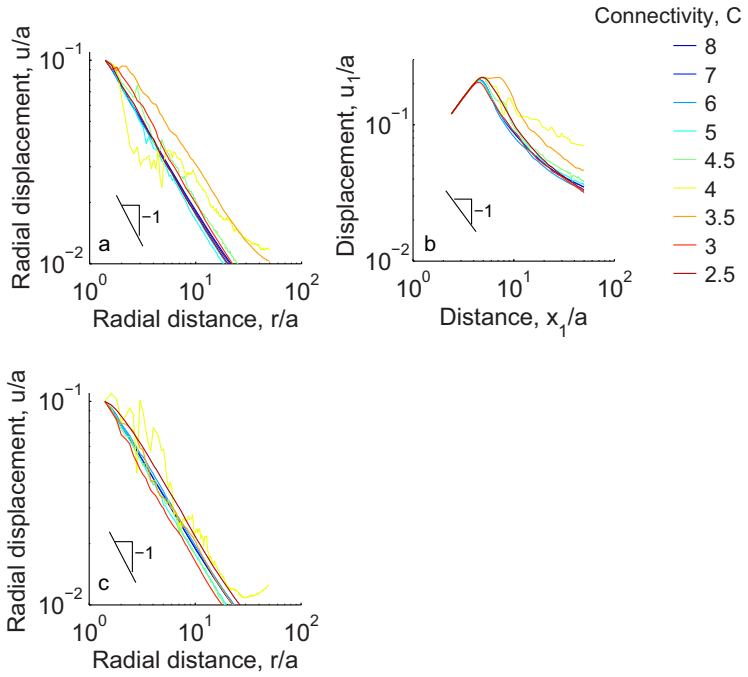

Figure S1: Simulated displacements for fibers that support compression, $\rho = 1$. (a) Displacements due to a contracting circle are computed with the bilinear (Fig. 2a) model with $\rho = 1$. The radial displacement component is averaged around circles of radius r from the origin and plotted. Results show displacement u vs. distance r for simulations that used connectivities ranging from $C = 2.5$ to $C = 8$. See Fig. 3b for the case of microbuckling, $\rho = 0.1$. (b) Displacements due to an ellipse with a ratio of semi-major to semi-minor axes $a_1/a_2 = 4$ with $\rho = 1$. The displacements u_1 along the major axis are plotted against distance along the axis x_1 for connectivities ranging from $C = 2.5$ to $C = 8$. See Fig. 4a for the case of microbuckling, $\rho = 0.1$. (c) Displacements due to a contracting circle computed with the strain stiffening model (Fig. 2b) with $\rho = 1$. As in (a), the radial displacement component is averaged around circles of radius r from the origin and plotted. See Fig. 3e for the case of microbuckling, $\rho = 0.1$. For all cases, typical slopes are -1 on logarithmic axes, indicate displacements scale according to the 2D linear elastic solution, $u \sim 1/r$.

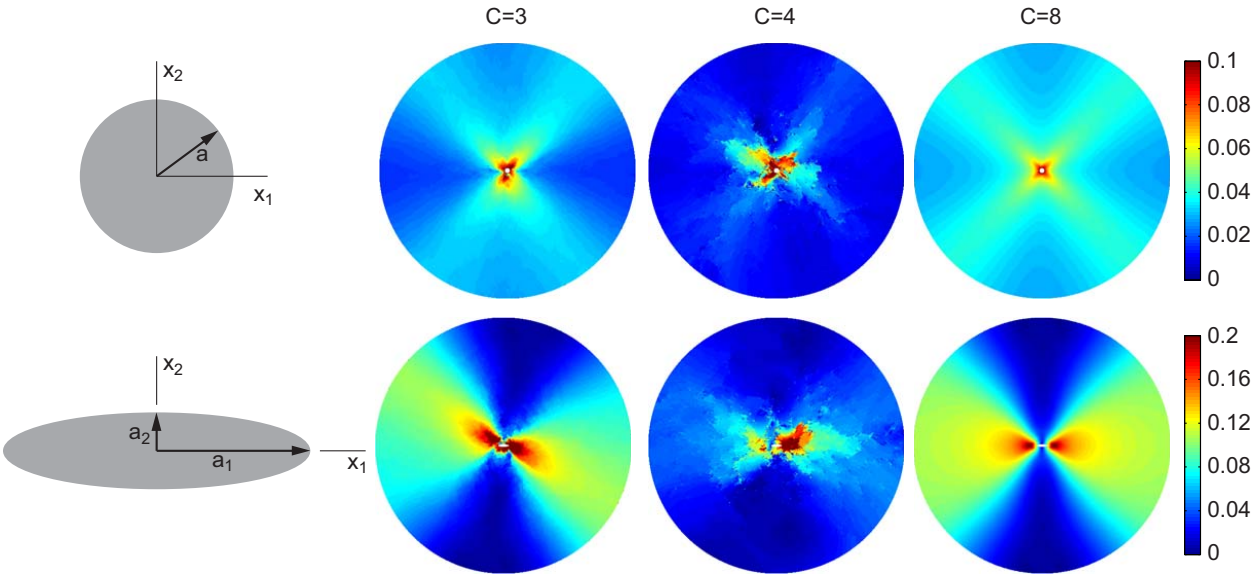

Figure S2: Displacements induced by a contracting circle and a contracting ellipse. A circle of radius a (top row) or an ellipse with semi-major and semi-minor axes a_1 and a_2 (bottom row) is simulated in a circular region with radius $b = 50a$. (For the ellipse, $a \equiv \sqrt{a_1 a_2}$.) For the circle, contractile displacements are applied uniformly around the perimeter, $u(r) = -0.1a$ at $r = a$ where $r = \left(x_1^2 + x_2^2\right)^{1/2}$. For the ellipse, contractile displacements are applied only along the major axis, $u_1(x_1) = -0.1a(x_1/a_1)$. The outer boundary $r = b$ is free of applied tractions. Microbuckling is simulated using the bilinear model with $\rho = 0.1$. Displacement magnitudes normalized by a are shown for the contracting circle and ellipse for connectivities C of 3, 4, and 8. Near the critical connectivity $C = 4$ large fluctuations in displacements occur for both the contracting circle and the ellipse, in agreement with previous models [31, 32]. These fluctuations are not present at lower ($C = 3$) or higher ($C = 8$) connectivities, where displacement fields are smoother.

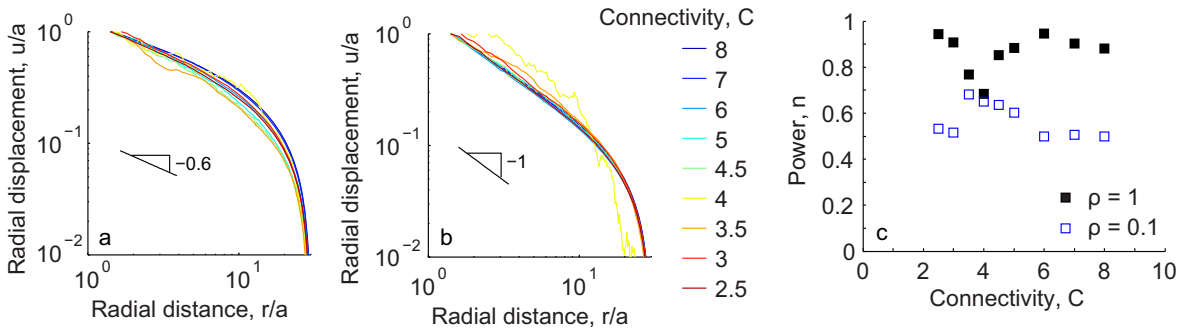

Figure S3: Effect of boundary conditions on simulation results. The simulations of Fig. 3 are repeated with fixed boundaries instead of free. (a) For elements with microbuckling ($\rho = 0.1$), displacements for all connectivities C have a slope of ~ -0.6 on logarithmic axes. (b) The simulations are repeated for elements without microbuckling ($\rho = 1$), and displacements have a slope of ~ -1 on a logarithmic scale. (c) For each connectivity, and for simulations with microbuckling ($\rho = 0.1$) and without ($\rho = 1$), displacements are fit to the linear elastic solution for a circular region of finite radius, $u = Ar^{-n} + Br^{n}$. (No fitting is performed to $u = Ar^{-n}$, because, as shown in (a) and (b), the fixed boundary affects the propagation of displacements for $r/a > 10$.) The fit power n is plotted for all cases. Similar to simulations with free boundaries (Fig. 3), simulations with microbuckling ($\rho = 0.1$) have lower powers of n, indicating displacements propagate over a long range when microbuckling is present.

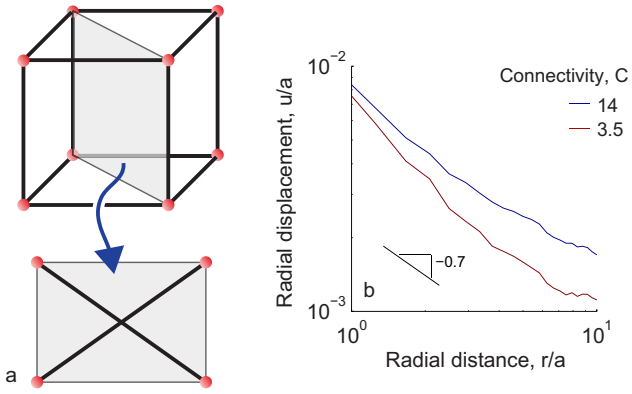

Figure S4: The displacements due to a contracting sphere in a fibrous matrix are simulated using a 3D model. $49 \times 49 \times 49$ nodes are used in a $20a \times 20a \times 20a$ region, where a is the radius of the sphere. A symmetric boundary is used at the bottom of the cubic region ($z = -10a$), and other boundaries are free. An inward displacement of $0.1a$ is applied to the nodes located at $r = a$. (a) Fiber connectivity. Each cube of 8 nodes is connected along the the cube's edges. Additionally, elements connect the diagonals as shown in the sketch. To simplify visualization, the sketch shows connections between only 2 diagonals, but the model connects all 4 diagonals with elements. As with the 2D models, lower connectivity is simulated by randomly selecting elements to delete. Deleted elements are replaced by weak elements with stiffness six orders of magnitude lower than that of the deleted elements. (b) Displacements due to the contracting sphere are averaged along circles of radius r from the center of the sphere in the x–y plane and plotted against radial distance for connectivities C of 3.5 (below the critical value of 6) and 14 (full connectivity). Fits to $u = Ar^{-n}$ give $n = 0.82$ and 0.67 for $C = 3.5$ and 14, respectively.

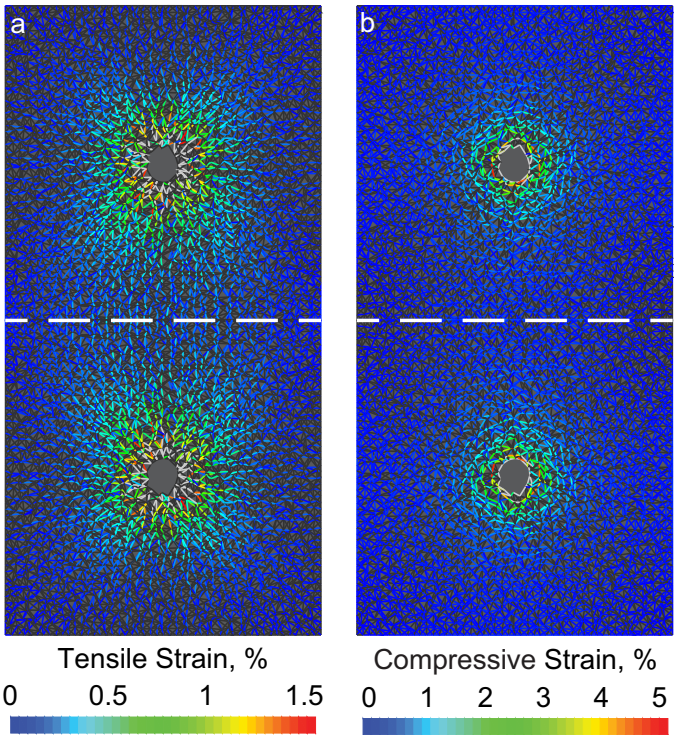

Figure S5: Tethers do not form when the matrix resists compression. Plots show tensile (a) and compressive (b) strains for the same simulation as in Fig. 5, but for fibers with equal stiffness in compression and tension ($\rho = 1$). Tensile strains (a) propagate radially outward from the contracting circle with no preferred directionality, and therefore no tethers form. Compressive strains (b) are roughly perpendicular to tensile strains.

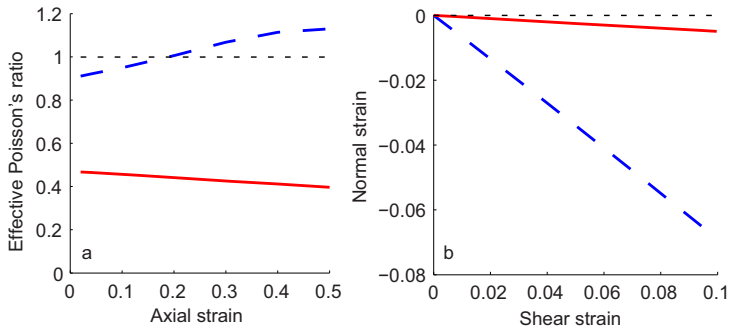

Figure S6: Microbuckling induces negative compressibility in tension and negative normal strains in shear. (a) The effective (engineering) Poisson's ratio is calculated in a uniaxial tension simulation for a model with matrix fibers that support compression ($\rho = 1$, solid red line) or buckle ($\rho = 0.1$, dashed blue line). In two dimensions, Poisson's ratios greater than 1 (dashed black line) indicate negative compressibility, in agreement with an experimental study on fibrin [11]. (b) Negative normal strains are observed in a simulation under shear loading for matrix fibers that support compression ($\rho = 1$, solid red line) or buckle ($\rho = 0.1$ dashed blue line). Similar to [10], negative normal strains are significantly larger for elements that simulate buckling. Simulations in this figure use the bilinear stress–strain relationship, but results are nearly identical for the WLC relationship. Results shown are for connectivity of $C = 8$.

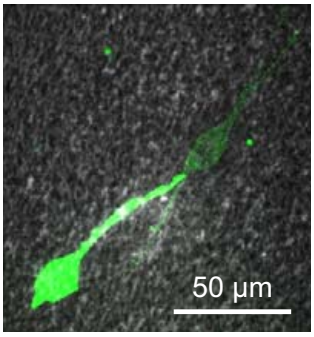

Figure S7: Pairs of fibroblast cells (green) in a 3D fibrin matrix (white) occasionally spread until they touch their neighbors. Image was captured with confocal microscopy 14 hrs after seeding the cells in the fibrin matrix.

Supplemental Data

Experimental data of 3D cell-induced displacements (Fig. 1b) for $n = 6$ cells are below. The data report the magnitude of cell-induced matrix displacements after averaging along different paths outward from the cell over time. For more details on how these cell-induced displacements are measured, see the methods section. The data set for each cell is displayed as an array of ordered pairs, (r,u) where each pair gives the distance from the cell's center r and the magnitude of the cell-induced matrix displacement u.

Cell 1. (25,0.68) (29,0.64) (33,0.61) (38,0.57) (42,0.53) (46,0.50) (50,0.47) (55,0.43) (59,0.40) (63,0.37) (67,0.35) (72,0.35) (76,0.38) (80,0.35)

Cell 2. (15,1.91) (20,1.78) (24,1.60) (28,1.42) (32,1.25) (36,1.15) (40,1.08) (44,1.01) (48,0.97) (52,0.90) (56,0.81) (60,0.69) (64,0.58) (68,0.53) (72,0.54)

Cell 3. (16,1.14) (21,1.04) (26,0.95) (31,0.89) (35,0.83) (40,0.77) (45,0.73) (49,0.70) (54,0.67) (59,0.66) (64,0.65) (68,0.64) (73,0.65)

Cell 4. (17,1.33) (22,1.22) (26,1.14) (31,1.07) (36,1.00) (41,0.95) (46,0.91) (51,0.87) (55,0.84)

Cell 5. (14,1.89) (18,1.60) (21,1.40) (25,1.30) (29,1.25) (32,1.21) (36,1.19) (40,1.17) (43,1.16) (47,1.14) (51,1.12)

Cell 6. (12,1.76) (16,1.66) (20,1.34) (24,1.25) (27,1.07) (31,1.18) (35,1.12) (39,1.08) (43,1.04) (46,0.99) (50,0.95) (54,0.92) (58,0.89) (61,0.86) (65,0.83)